

Induction heating of cylindrical nonmagnetic ingots by rotation in static magnetic field generated by permanent magnets

ARTICLE INFO

Article history:

Received 27 September 2011

Received in revised form 21 February 2012

Keywords:

Induction heating

Permanent magnets

Monolithic formulation

Numerical analysis

Higher-order finite element method

Adaptivity

ABSTRACT

Induction heating of cylindrical nonmagnetic billets by their rotation in static magnetic field is modeled. The magnetic field is produced by a system of appropriately arranged permanent magnets. The numerical model is solved by our own full adaptive higher-order finite element method in a monolithic formulation, i.e., both magnetic and temperature fields are solved simultaneously, respecting their mutual interaction. All principal nonlinearities are included in the model (permeability of ferromagnetic parts of the system as well as temperature dependences of physical parameters of the heated metal). The methodology is illustrated by two examples whose results are discussed.

© 2012 Elsevier B.V. All rights reserved.

1. Introduction

Induction heating of cylindrical billets of various nonmagnetic metals (mostly aluminum) is a widespread technological process often used for their softening before hot forming [1,2]. This process is usually realized by the two following manners:

- heating of an unmoving billet in a system of static, harmonic currents carrying inductors,
- heating of a rotating billet in static magnetic field generated by static coils.

Heating by inductors carrying harmonic currents belongs to the classical ways of such heat treatment (the simplest possible arrangement is schematically shown in Fig. 1) that has been employed since the thirties of the twentieth century. But its effectiveness is rather low due to the high Joule losses in the inverter and inductor (that must be transferred away by an appropriate cooling medium). The efficiency of the process typically does not exceed 40%–50%. More details about the process and its modeling can be found in numerous publications; see, e.g., [3–6].

Heating of a rotating billet in static magnetic field produced by direct current-carrying inductor is schematically depicted in Fig. 2. It was proposed about ten years ago and modeled by several groups of authors [7–10]. But even here we have to face serious problems. The most important of them is generation of a sufficiently high magnetic field and corresponding eddy currents in the billet. As its revolutions are rather limited (in the case of massive billets with diameters over 0.1 m their value $n = 750$ rpm or, at most, 1500 rpm), the only possible solution is using very high field currents, which usually requires superconducting devices with all necessary amenities. Now the Joule losses (due to a low resistance of the field windings) are not so significant, but certain energy is consumed by the cooling devices and rotation of the billet. The overall efficiency of the process is reported to be about 70%–80%. Presently, several systems of this kind successfully work in industrial plants, such as [11].

The authors of this paper started with research of another version of this method suitable for billets of lower diameters, up to about 0.1 m. Here the static magnetic field is generated by appropriately arranged high-parameter permanent magnets.

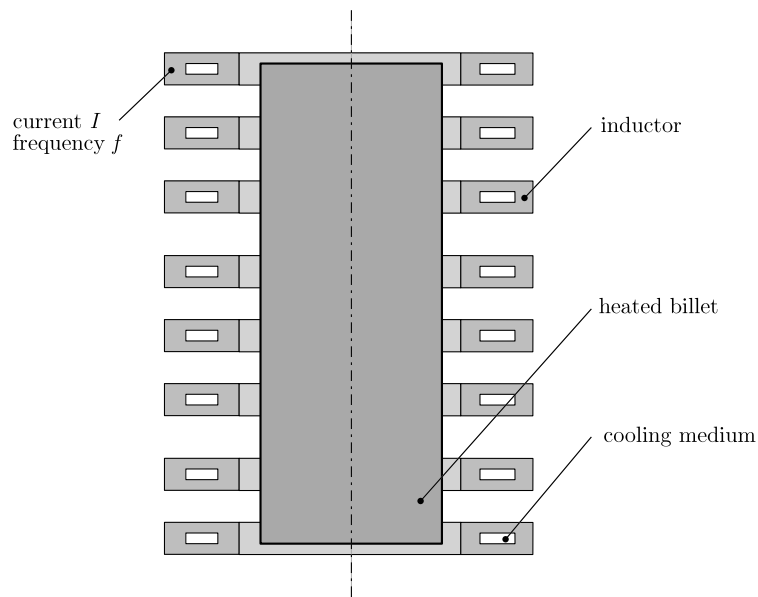


Fig. 1. Induction heating of a static metal billet in a static inductor carrying harmonic current of amplitude I and frequency f .

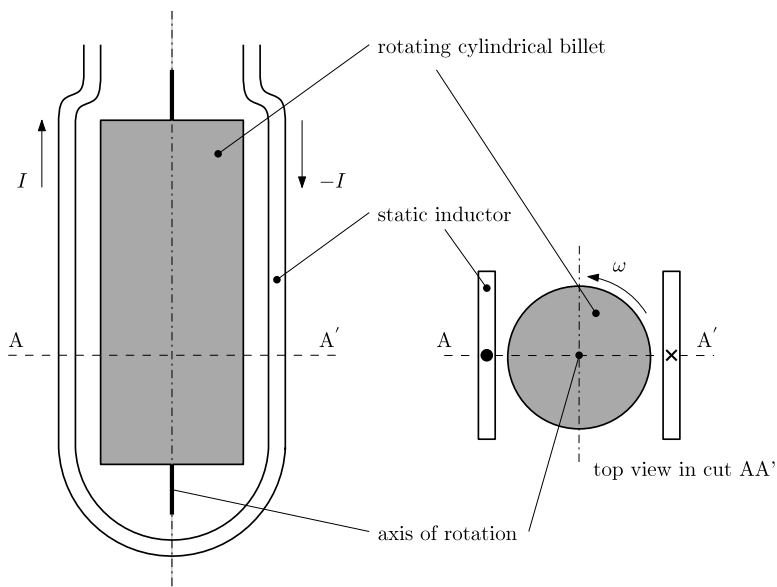


Fig. 2. Induction heating of a rotating metal billet in a static inductor carrying direct current of value I .

This version is characterized by the absence of the field coils (and corresponding Joule losses) and the only losses in the system are mechanical. The driving engine must provide a torque higher than the drag torque caused by the interaction between the static magnetic field and currents induced in the rotating billet. In this case, efficiency could reach even 85%. The first study of the system describing induction heating of a thin-wall aluminum pipe was published in [12,13], and several results were validated (with a very good agreement) experimentally on a physical model.

The paper deals with a thorough analysis of the induction heating of massive aluminum billets realized in this manner. Determined are the main operation characteristics of the process such as the velocity of heating, drag torque, efficiency, and other quantities of higher importance.

2. Formulation of technical problem

Two versions of the investigated arrangement are depicted in Figs. 3 and 4. They are sufficiently long in the axial direction, so that the distributions of magnetic and temperature fields in them may be considered 2D. The aluminum billet rotates (at

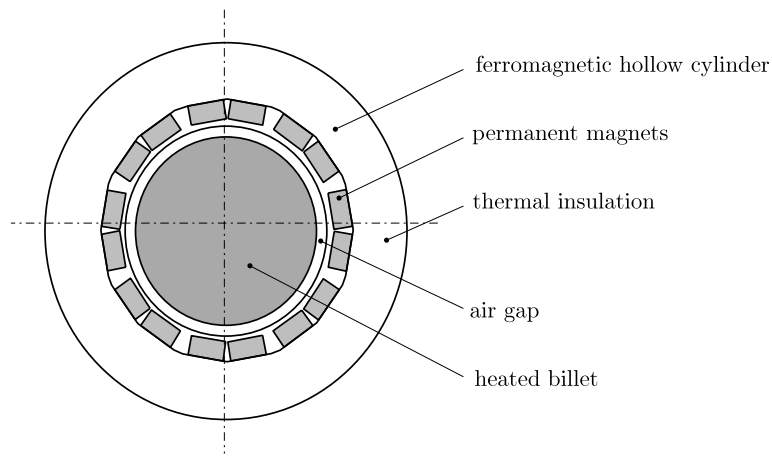


Fig. 3. Arrangement with permanent magnets fixed on a ferromagnetic hollow cylinder.

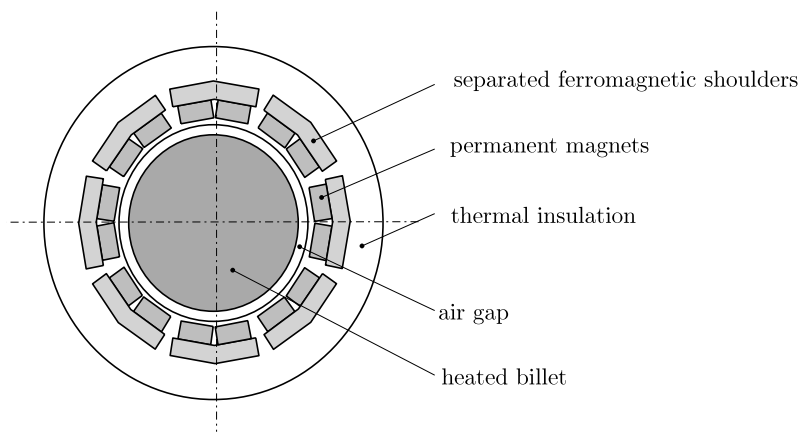


Fig. 4. Arrangement with permanent magnets fixed on ferromagnetic shoulders.

angular velocity ω) in the static part of the system consisting of permanent magnets fixed either in a ferromagnetic hollow cylinder (Fig. 3), or on ferromagnetic shoulders (Fig. 4). The permanent magnets are embedded in a good thermal insulation that prevents them from excessive heating due to convection of heat from the billet.

The number of permanent magnets in Fig. 3 should be even (due to magnetic symmetry) while the number of the shoulders carrying a pair of such magnets can be quite arbitrary. Orientation of the permanent magnets is not depicted in this general scheme because it can change from one case to another case.

The goal is to map the distribution of magnetic field in the system and time evolution of its local and average temperatures. In addition to finding its principal characteristics, checked will also be the temperature rise of the permanent magnets that must not exceed a prescribed value (higher temperature could substantially deteriorate their operation parameters). The problem is solved in the monolithic formulation (i.e., both physical fields are solved simultaneously, with one stiffness matrix). All important nonlinearities of the system are taken into account.

3. Continuous mathematical model of the problem

Magnetic field in the system may advantageously be described by the magnetic vector potential \mathbf{A} . Its distribution is given by the solution of the equation [14]

$$\operatorname{curl} \left(\frac{1}{\mu} \operatorname{curl} \mathbf{A} - \mathbf{H}_c \right) - \gamma \mathbf{v} \times \operatorname{curl} \mathbf{A} = \mathbf{0}, \quad (1)$$

where γ is the electrical conductivity, μ denotes the magnetic permeability, \mathbf{v} stands for the vector of the local velocity of rotation, and \mathbf{H}_c is the coercive force (this is only considered in the domain of the permanent magnets, elsewhere it vanishes). A sufficiently distant artificial boundary is described by the Dirichlet condition $\mathbf{A} = \mathbf{0}$.

The currents induced in the rotating billet are characterized by the density

$$\mathbf{J}_{\text{ind}} = \gamma \mathbf{v} \times \operatorname{curl} \mathbf{A} \quad (2)$$

that produces in it the volumetric Joule losses

$$w_J = \frac{\|\mathbf{J}_{\text{ind}}\|^2}{\gamma}. \tag{3}$$

These losses represent the local sources of heat.

The time-dependent distribution of the temperature in the system obeys the heat transfer equation in the form [15]

$$\text{div} (\lambda \text{grad } T) = \rho c \cdot \left(\frac{\partial T}{\partial t} + \mathbf{v} \cdot \text{grad } T \right) - w_J, \tag{4}$$

where λ is the thermal conductivity, ρ denotes the specific mass, and c stands for the specific heat. The boundary condition along the external surface S of the system can be written in the form

$$-\lambda \frac{\partial T}{\partial n} = \alpha_{\text{gen}}(T_S - T_0), \tag{5}$$

where α_{gen} stands for the generalized coefficient of convective heat transfer that includes also the influence of radiation, T_S is the surface temperature, T_0 is the ambient temperature and n denotes the direction of the outward normal to the surface of the system at a given point.

All physical parameters of used materials ($\mu, \gamma, \lambda, \rho, c$) are generally nonlinear functions of temperature T and these nonlinearities (as far as they are known) are respected. Temperature-dependent is also the coefficient α_{gen} , but this dependence is very difficult to find, so that it will be considered constant.

Eqs. (1) and (4) together with the corresponding boundary and initial conditions will be solved numerically, in a monolithic formulation.

4. Numerical solution

The solution of (1) and (4) is realized in the Cartesian coordinates x, y . First, both equations are transformed in the sense of the weak formulation. The form corresponding to (1) reads

$$\begin{aligned} & \int_{\Omega} \frac{1}{\mu} \left(\frac{\partial A_z}{\partial x} \cdot \frac{\partial w}{\partial x} + \frac{\partial A_z}{\partial y} \cdot \frac{\partial w}{\partial y} \right) dS + \int_{\Omega} \gamma \left(A_z v_x \cdot \frac{\partial w}{\partial x} + A_z v_y \cdot \frac{\partial w}{\partial y} \right) dS \\ & = - \int_{\Omega} \frac{1}{\mu} \left(B_{r,y} \cdot \frac{\partial w}{\partial x} - B_{r,x} \cdot \frac{\partial w}{\partial y} \right) dS - \int_{\Gamma} K \cdot w dl, \end{aligned} \tag{6}$$

while the analogous form for (4) is

$$\begin{aligned} & \int_{\Omega} \lambda \left(\frac{\partial T}{\partial x} \cdot \frac{\partial w}{\partial x} + \frac{\partial T}{\partial y} \cdot \frac{\partial w}{\partial y} \right) dS + \int_{\Omega} \rho c \frac{\partial T}{\partial t} \cdot w dS \\ & - \int_{\Omega} \rho c T \left(v_x \cdot \frac{\partial w}{\partial x} + v_y \cdot \frac{\partial w}{\partial y} \right) dS + \int_{\Gamma} \alpha T \cdot w dl \\ & = \int_{\Omega} w_J \cdot w dS + \int_{\Gamma} (\alpha T_0 + g) \cdot w dl. \end{aligned} \tag{7}$$

Here, Ω denotes the cross section of the investigated area and Γ is its boundary. Symbol A_z is the z -component of magnetic vector potential, v_x and v_y are the components of velocity \mathbf{v} in the corresponding directions, and, finally, $B_{r,x}$ and $B_{r,y}$ stand for the components of remanence \mathbf{B}_r . Symbol α denotes the generalized coefficient of convective heat transfer, T_0 is temperature of external air, and K and g are appropriate constants. Finally, w is a suitable testing function of a polynomial character satisfying the boundary conditions of the problem.

The numerical solution of (6) and (7) is realized by a fully adaptive higher-order finite element method [16], whose algorithms are implemented into our own codes Hermes [17] and Agros2D [18]. Both codes have been developed in our group for a couple of years.

The codes written in C++ are intended for monolithic numerical solution of systems of generally nonlinear and nonstationary second-order partial differential equations (rewritten into corresponding weak formulations), whose principal purpose is modeling of complex coupled physical problems. While Hermes is a library containing the most advanced procedures and algorithms for the numerical processing of the task, Agros2D represents a powerful preprocessor and postprocessor. Both codes are freely distributable under the GNU General Public License. The most important (and often quite unique) features of the codes follow:

- Solution of the system of PDEs is carried out monolithically, which means that the resultant numerical scheme is characterized by just one stiffness matrix. The PDEs are first rewritten into the weak forms whose numerical integration provides its coefficients. The integration is performed using the Gauss quadrature formulas.

- Fully automatic *hp*-adaptivity. In every iteration step the solution is compared with the reference solution (realized on an approximately twice finer mesh), and the distribution of error is then used for selection of candidates for adaptivity. Based on sophisticated and subtle algorithms the adaptivity is realized either by a subdivision of the candidate element or by its description by a polynomial of a higher order [16]. The mesh can be composed of triangular, quadrilateral or curved elements and their combination.
- Each physical field can be solved on quite a different mesh that best corresponds to its particulars. This is of great importance, for instance, for respecting skin effect in the electromagnetic field, boundary layers in the problems containing the field of flow, etc. Special powerful higher-order techniques of mapping are then used to avoid any numerical errors in the process of assembly of the stiffness matrix. In nonstationary processes every mesh can change in time, in accordance with the real evolution of the corresponding physical quantities.
- Easy handling with hanging nodes [19] appearing on the boundaries of subdomains whose elements have to be refined. Usually the hanging nodes bring about a considerable increase of the number of the degrees of freedom (DOFs). The code contains higher-order algorithms for respecting these nodes without any need of an additional refinement of the external parts neighboring with the refined subdomain.

The algorithms of adaptivity start to be applied at the moment when some local error of solution is higher than the acceptable tolerance. Consider an equation

$$Lf = 0 \quad (8)$$

where L denotes a differential operator and f a function whose distribution over some domain is to be found. If f' is its approximation obtained by numerical solution of (8), the absolute and percentage relative errors η and ε are defined by the relations

$$\eta = f - f', \quad \varepsilon = 100 \left| \frac{\eta}{f} \right|. \quad (9)$$

Other quantities that can be checked in this way are the norms. Hermes2D, for example, works with the basic energetic norm given by the expression

$$\|e\| = \left| \int_{\Omega} \eta(L\eta) \, d\Omega \right|^{1/2}. \quad (10)$$

L^2 norm defined by the relation

$$\|e\|_{L^2} = \left| \int_{\Omega} \eta^2 \, d\Omega \right|^{1/2}, \quad (11)$$

and H^1 norm given by the expression

$$\|e\|_{H^1} = \left| \int_{\Omega} (\eta^2 + \text{grad } \eta \cdot \text{grad } \eta) \, d\Omega \right|^{1/2}. \quad (12)$$

Unfortunately, the exact solution f is known only in very simple analytically solvable cases. Moreover, there exists no general method that would provide a good estimation of the error for an arbitrary PDE. That is why the codes work [16] with the reference solution f_{ref} instead, that is obtained either by a refinement of the whole mesh (*h*-adaptivity), by enlargement of the polynomial degree (*p*-adaptivity) or by both above techniques (*hp*-adaptivity). In this manner we get the candidates for adaptivity even without knowledge of the exact solution f . The library Hermes2D works with very sophisticated and subtle higher-order tools based on the above considerations.

5. Illustrative examples

The first example solves an arrangement corresponding to Fig. 5. A cylindrical aluminum billet of diameter $d = 60$ mm is inductively heated by rotation at a given angular frequency corresponding to $n = 1500$ rpm in a stationary magnetic field generated by a system of permanent magnets, see Fig. 6. The axial length of the arrangement is 500 mm.

The magnetic circuit is made of standard carbon steel ČSN 12 040. Its material characteristics are depicted in Figs. 7–10. Fig. 7 shows its magnetization characteristic at the room temperature ($T_0 = 20$ °C). But this information is not enough. Magnetic permeability μ_r , as known, is a function of magnetic flux density B and temperature T . For every type of steel this function must be found experimentally, which usually represents a serious complication. We introduce, therefore, an assumption that $\mu_r(B, T) = \mu_r(B, T_0) \cdot \varphi(T)$, where $\mu_r(B, T_0)$ is the dependence of relative permeability on magnetic flux density B at a given temperature T_0 and function φ is given by the relation

$$\begin{aligned} \text{for } T_0 \leq T \leq T_C \quad \varphi(T) &= a - bT^2, \\ \text{for } T_C \leq T \quad \varphi(T) &= \frac{1}{\mu_r(B, T_0)}. \end{aligned}$$

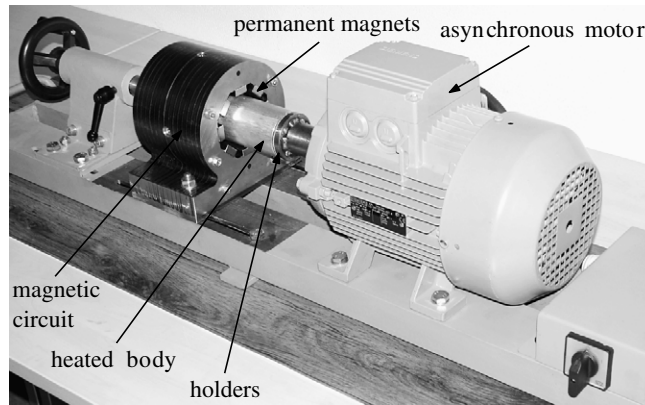


Fig. 5. Experimental device.

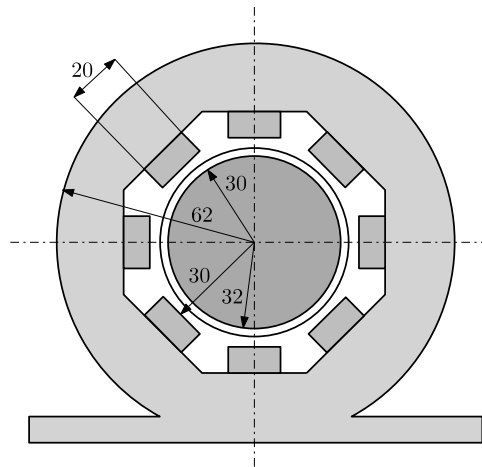


Fig. 6. Cylindrical aluminum billet rotating in a system of permanent magnets (all dimensions in mm).

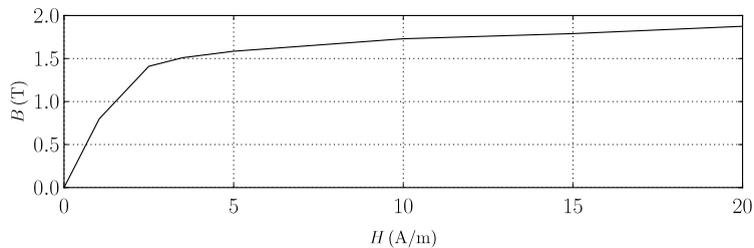


Fig. 7. Magnetization characteristic of steel 12 040.

Here

$$a = \frac{\mu_r(B, T_0)T_C^2 - T_0^2}{\mu_r(B, T_0)(T_C^2 - T_0^2)}, \quad b = \frac{\mu_r(B, T_0) - 1}{\mu_r(B, T_0)(T_C^2 - T_0^2)},$$

and T_C is the Curie temperature (for the steel used its value is approximately 800 °C).

Figs. 8–10 show the temperature dependences of its electrical conductivity, thermal conductivity and heat capacity, respectively. Obviously, all of them are nonlinear.

The permanent magnets (based on rare earths) are of type VMM10 and exhibit the remanence $B_r = 1.41$ T and relative permeability in the second quadrant $\mu_r = 1.21$. They are the strongest magnets available in our market.

Figs. 11–13 show the temperature-dependent characteristics of pure aluminum. Even those exhibit nonlinear behavior.

Thermal insulation is made of glass wool that exhibits very good insulation properties. Its thermal conductivity is considered independent of temperature and its value $\lambda = 0.04$ W/mK and even its thin layer prevents the permanent magnets from excessive overheating.

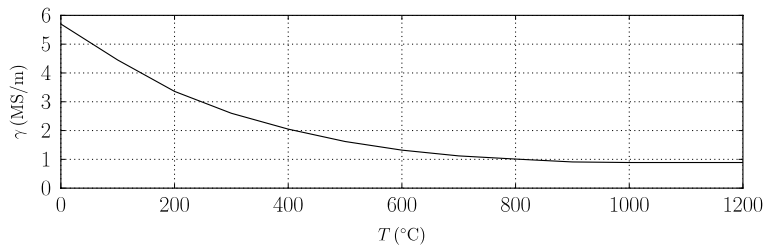


Fig. 8. Dependence of $\gamma = \gamma(T)$ for steel 12 040.

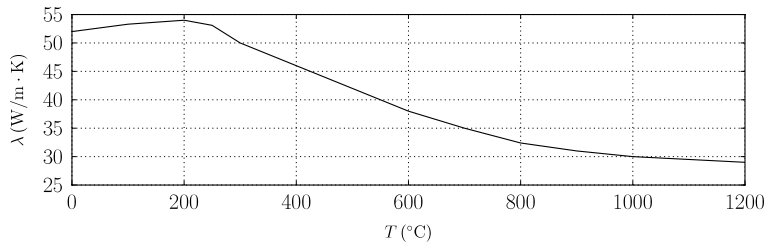


Fig. 9. Dependence of $\lambda = \lambda(T)$ for steel 12 040.

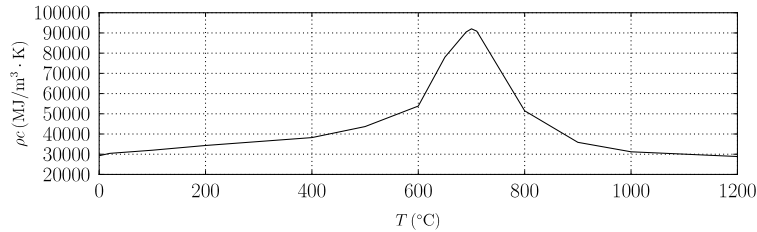


Fig. 10. Dependence of $\rho c = \rho c(T)$ for steel 12 040.

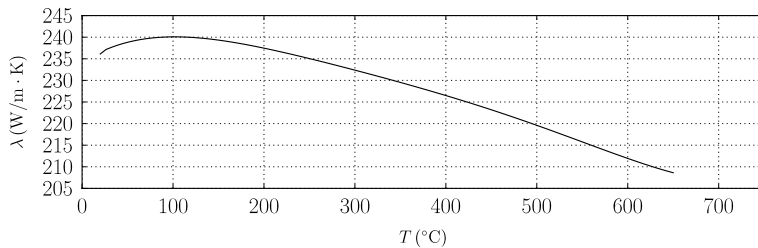


Fig. 11. Dependence of $\lambda = \lambda(T)$ for aluminum.

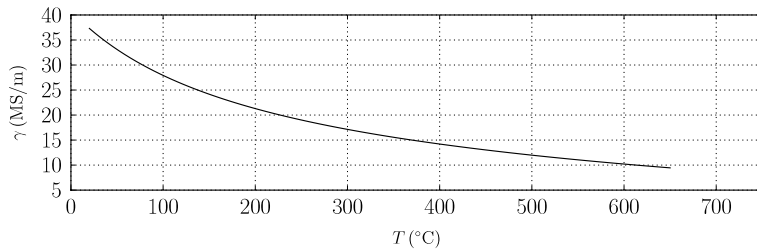


Fig. 12. Dependence of $\gamma = \gamma(T)$ for aluminum.

First, a series of computations showed that both permanent magnets and magnetic circuit remain practically cold (even when the average temperature of the billet was more than 300 °C, their temperature did not exceed about 40 °C). This allowed accepting an assumption that the physical parameters of these parts may be considered independent of temperature, which simplified all remaining calculations, shortening them several times.

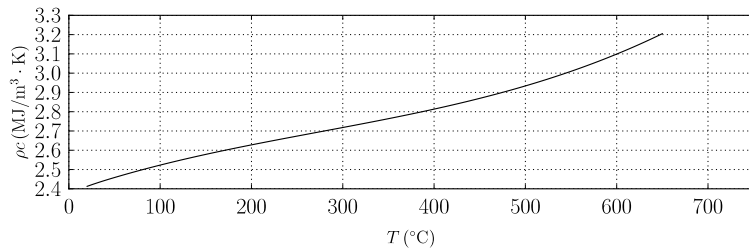


Fig. 13. Dependence of $\rho_c = \rho_c(T)$ for aluminum.

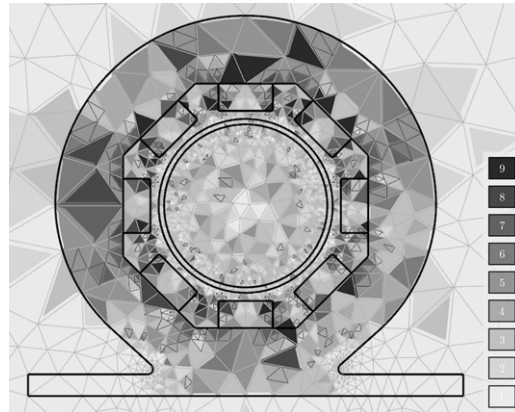


Fig. 14. Mesh for the computation of magnetic field in the system.

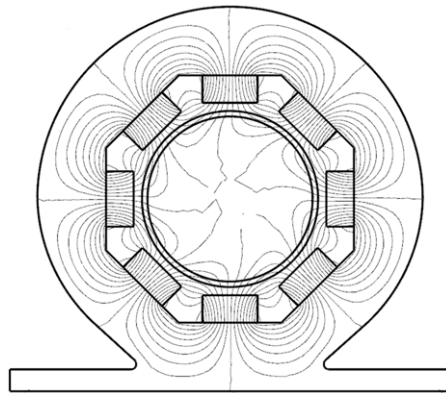


Fig. 15. Distribution of magnetic field calculated on the mesh in Fig. 14.

Fig. 14 shows the discretization mesh used for modeling of magnetic field in the system after several adaptive steps. The mesh combines triangular and curved elements, which leads to savings in about 20% of DOFs compared with a purely triangular mesh (the accuracy of results being the same). The numbers in rectangles on the right side show the orders of polynomials in particular elements. Fig. 15 shows the corresponding distribution of magnetic field in the system.

Fig. 16 shows the convergence curves (dependences of the relative error of magnetic field on the number of DOFs) for a mesh with purely triangular elements and with combined elements, when the process of adaptivity starts either from linear ($p = 1$) or quadratic ($p = 2$) polynomials. The computations on the with combined elements obviously converge faster.

The distribution of temperature along the radius of the billet within the range 0–25 mm for several time levels is shown in Fig. 17. This distribution is practically quite uniform, which is caused by a very good thermal conductivity of pure aluminum and relatively long period of heating (on the order of minutes). Of course, some minor front effects can be expected at both ends of the billet, but our previous experimental experience confirmed that they were very small (below about 3%).

Finally, Fig. 18 depicts the time dependence of the average temperature in the billet. This dependence is almost linear, which shows that the process of heating is practically adiabatic. This is caused by the small thickness of the air gap, a good thermal insulation, and sufficient length of the system.

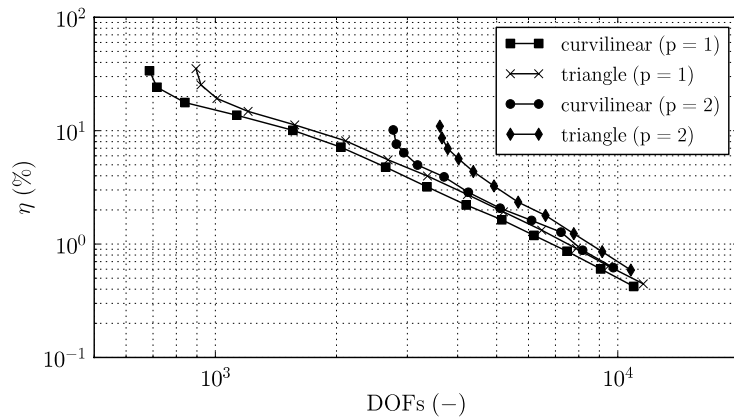


Fig. 16. Convergence curves of computation of magnetic field in the system.

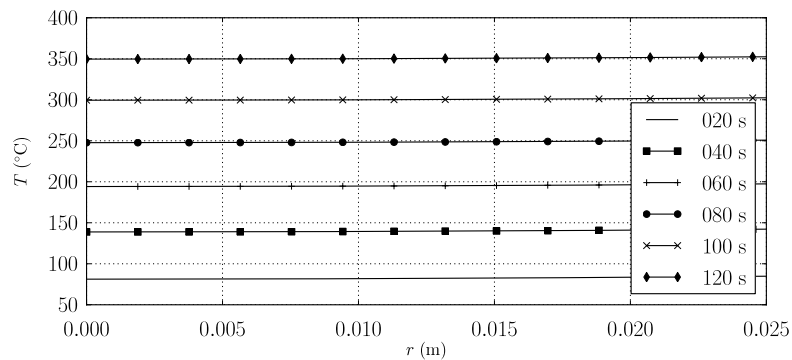


Fig. 17. Distribution of the temperature along the radius of the billet for several time levels.

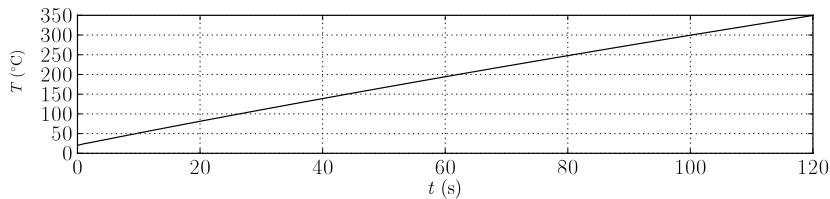


Fig. 18. Time evolution of the average temperature of the billet.

The second example solves another arrangement corresponding to Fig. 4. A cylindrical aluminum billet of diameter $d = 100$ mm is inductively heated by rotation at a given angular frequency corresponding to $n = 750$ rpm, see Fig. 20. The number of shoulders with one pair of permanent magnets is 8. The axial length of the arrangement is 120 mm. All materials have the same parameters as in the previous example.

The task is to map the process of heating and its parameters in the dependence on the thickness δ of air gap that may change from 10 to 1 mm.

We considered two possible variants differing by the orientation of permanent magnets according to Fig. 19.

First, we investigated the convergence of results for the distribution of magnetic field at the initial temperature (20°C). The corresponding graphs for the variant b are in Figs. 21 and 22. While Fig. 21 shows the dependence of the relative error of computation on the number of DOFs, Fig. 22 depicts the dependence of the same value on the number of the adaptive steps.

While application of h -adaptivity for $p = 1$ (first-order polynomials) lead to a very slow convergence, for $p = 2$ the situation is much more favorable. But the fastest convergence is obtained for the p -adaptivity and full hp -adaptivity. Within the range of the depicted errors both curves are practically identical.

Fig. 23 shows the final discretization mesh (variant b) after the adaptive process. The numbers in rectangles on the right depict the orders of the polynomials approximating the magnetic vector potential in particular elements.

Fig. 24 depicts the dependence of the average volumetric Joule losses in the billet on the thickness δ of the gap. It is obvious that from this viewpoint variant b is much more favorable.

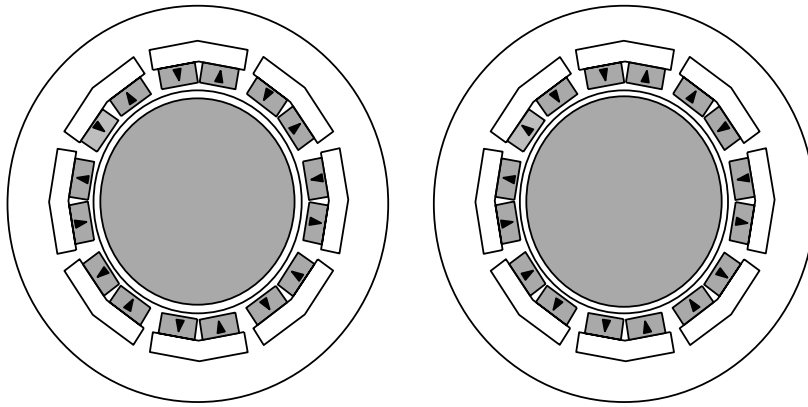


Fig. 19. Two variants differing by the orientation of the permanent magnets.

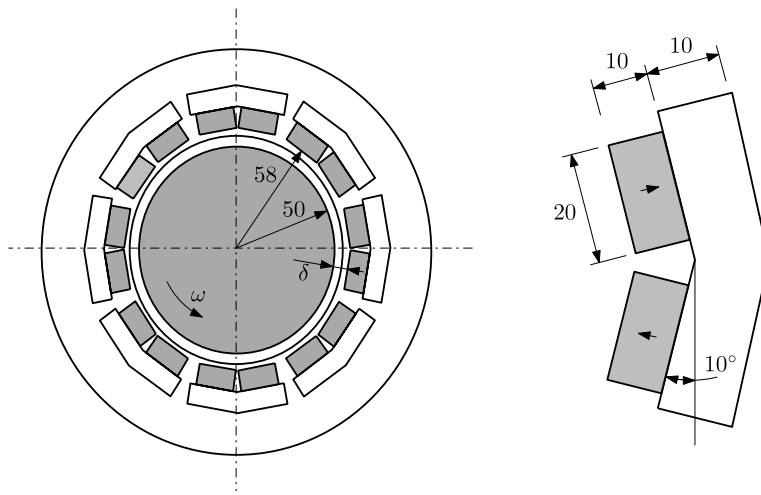


Fig. 20. The solved arrangement with the detail of the shoulder (dimensions in mm).

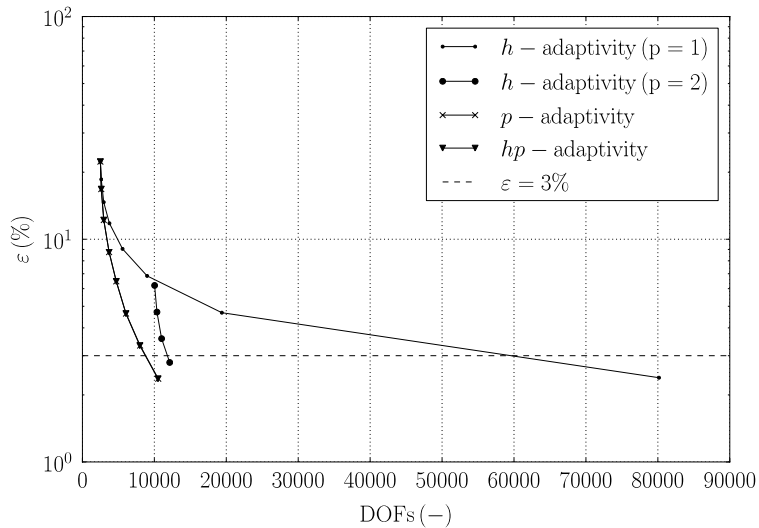


Fig. 21. Dependence of relative error ε on the number of DOFs (magnetic field, variant b).

Figs. 25 and 26 show the time evolution of the average temperature of the billet for variants a and b , respectively, for variable thickness δ of the gap between the permanent magnets and billet. With decreasing thickness δ the process of heating

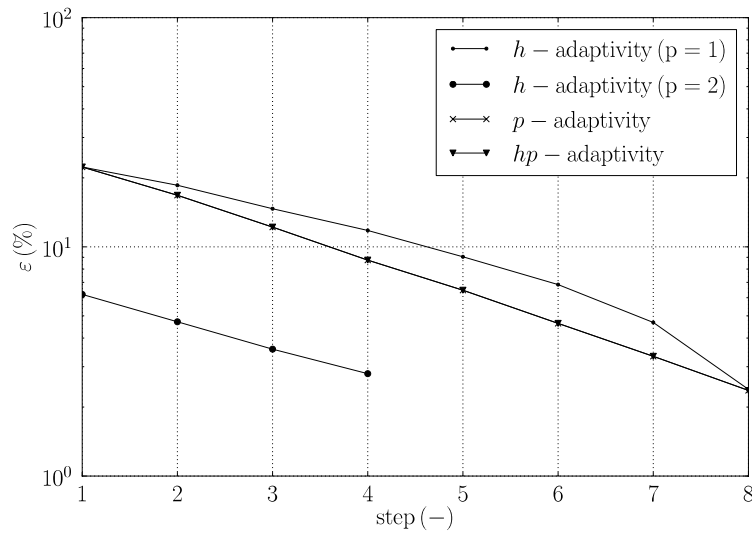


Fig. 22. Dependence of relative error ε on the number of iterative steps (magnetic field, variant b).

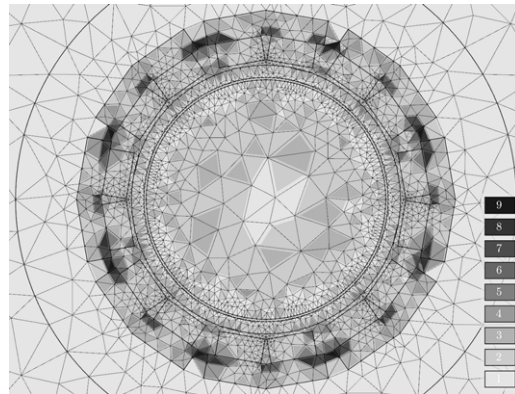


Fig. 23. Discretization mesh used for the computation (magnetic field, variant b) (number of elements is 4 751, number of DOFs is 10 832).

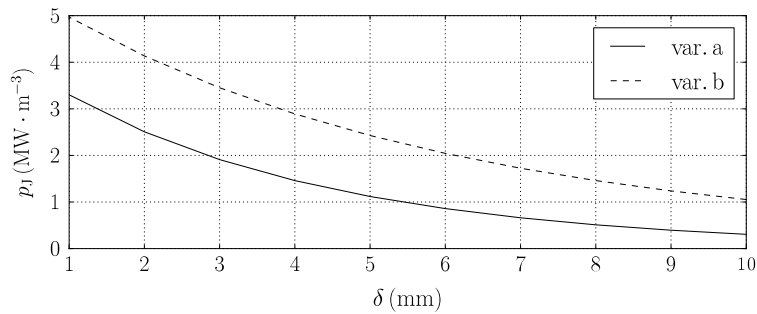


Fig. 24. Dependence of the average volumetric Joule losses in the billet on the thickness δ of the gap.

is faster. But small values of δ are practically unreal. This would lead to a very thin layer of thermal insulation and subsequent danger of overheating the permanent magnet. Necessary is, therefore, a suitable compromise.

Fig. 27 depicts the drag torque T_d per 1 m of the billet as a function on the thickness δ of the gap. It is obvious that the interaction of the magnetic field produced by the permanent magnets with the billet grows with decreasing value of δ . This is, as shown in the previous figure, more favorable from the viewpoint of the velocity of heating, but the power of the driving engine must be higher.

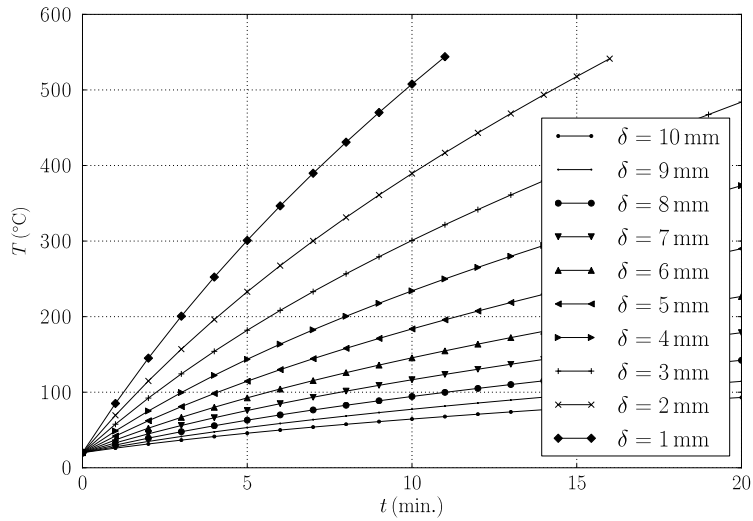


Fig. 25. Time evolution of the average temperature of the billet for variable thickness δ of the gap (variant a).

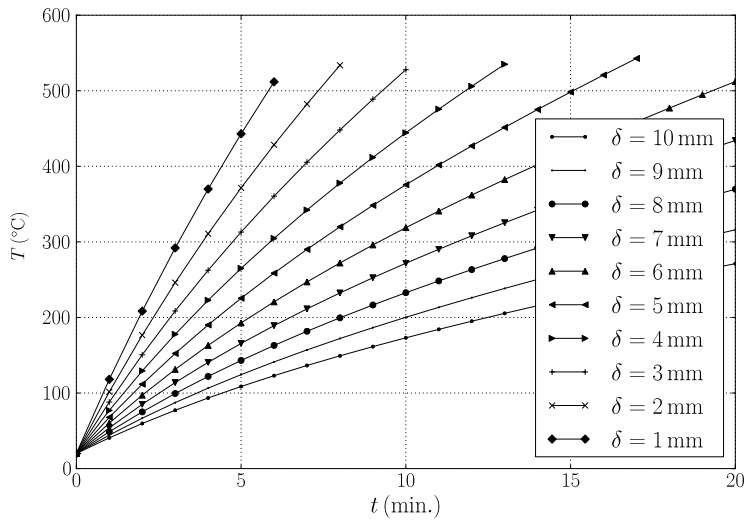


Fig. 26. Time evolution of the average temperature of the billet for variable thickness δ of the gap (variant b).

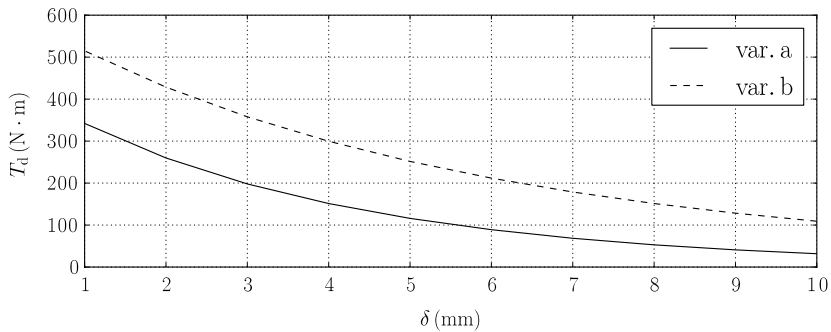


Fig. 27. Dependence of the drag torque T_d produced by the system on the thickness δ of the gap.

The last important quantity is the efficiency η of the process. It can be determined from the value

$$\eta = \frac{Q}{W_m},$$

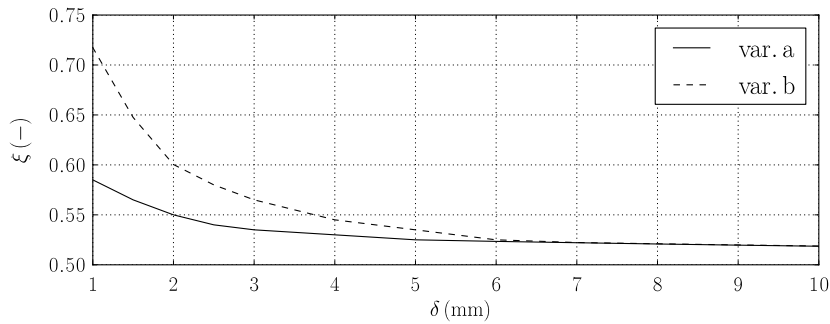


Fig. 28. Dependence of efficiency ξ of the process on the thickness δ of the gap.

where Q is heat delivered to the billet and W_m denotes the mechanical energy spent for rotation. While Q may be determined as

$$Q = mc(T - T_0) = \rho cV(T - T_0),$$

the mechanical energy W_m delivered to the system is

$$W_m = T_d \omega t_T.$$

Here, ρc is the heat capacity of aluminum, V is the volume of the billet, ω is the angular velocity, and T_0 is its initial temperature. Finally, t_T is the time in which the average temperature of the billet reaches the chosen value T . Fig. 28 shows the dependence of efficiency ξ on the thickness δ of the gap. It is clear that with decreasing thickness δ of the gap the efficiency increases. The reason is higher magnetic flux penetrating into the heated billet.

6. Conclusion

The fully adaptive higher-order finite element method used for modeling of the described problem represents a powerful and precise tool for numerical solution of complex physical phenomena. The model provided realistic results and shows that even relatively massive billets may successfully be heated by their rotation in magnetic field produced by a system of permanent magnets.

Next work in the field must be aimed at the optimization techniques that would lead to the design of the most advantageous arrangements (including orientation of the permanent magnets) from the viewpoint of the velocity of heating, drag torque and overall efficiency of the system. The principal way consists in considering a thinner gap between the billet and permanent magnets, on the other hand, there must still be place enough for the thermal insulation.

Acknowledgment

This work was supported by the European Regional Development Fund and Ministry of Education, Youth and Sports of the Czech Republic under the project No. CZ.1.05/2.1.00/03.0094 RICE, by the Grant project P102/11/0498 (GACR), Grant project P102/10/0216 (GACR) and Research Plan MSM 6840770017.

References

- [1] P. Cavaliere, Hot and warm forming of 2618 aluminum alloy, *Journal of Light Metals* 2 (2002) 247–252.
- [2] J.R. Davies, *Aluminum and Aluminum Alloys*, ASM International, Handbook Committee, 1993.
- [3] E.J. Davies, *Conduction and Induction Heating*, P. Peregrinus Ltd., London, 1990.
- [4] I. Rudnev, V., D. Loveless, R. Cook, M. Black, *Handbook of Induction Heating*, Marcel Dekker, Inc., New York, 2003.
- [5] S. Zinn, S.L. Semiatin, *Elements of Induction Heating: Design, Control and Applications*, ASM International, 1988.
- [6] E. Rapoport, Y. Pleshivtseva, *Optimal Control of Induction Heating Process*, CRC Press, Boca, 2006.
- [7] N. Magnusson, R. Bersas, M. Runde, Induction heating of aluminium billets using hts dc coils, *Institute of Physics Conference Series* (2004) 1104–1109.
- [8] R. Araneo, F. Dughiero, M. Fabbri, M. Forzan, A. Geri, A. Morandi, S. Lupi, P.L. Ribani, G. Veca, Electromagnetic and thermal analysis of the induction heating of aluminium billets rotating in dc magnetic field, *COMPEL* 27 (2008) 467–479.
- [9] M. Fabbri, A. Morandi, L. Ribani, Dc induction heating of aluminum billets using superconducting magnets, *COMPEL* 27 (2008) 480–490.
- [10] M. Fabbri, S. Lupi, A. Morandi, L. Ribani, Experimental and numerical analysis of dc induction heating of aluminum billets, *IEEE Transactions on Magnetics* 45 (2009) 192–200.
- [11] Weseralu gmbh & co. kg, am osthafen 5, 32423 minden. URL <http://www.weseralu.de>.
- [12] P. Karban, F. Mach, I. Doležel, Induction heating of nonmagnetic cylindrical billets by rotation in magnetic field produced by static permanent magnets, *Przeglad Elektrotechniczny (Electrical Review)* 86 (2010) 53–56.
- [13] P. Karban, F. Mach, I. Doležel, J. Barglik, Higher-order finite element modeling of rotational induction heating of nonferromagnetic cylindrical billets, *COMPEL* 30 (2009) 1517–1527.
- [14] M. Kuczmann, A. Iványi, *The Finite Element Method in Magnetics*, Akademiai Kiadó, Budapest, 2008.
- [15] J.P. Holman, *Heat Transfer*, McGraw Hill, NY, 2002.
- [16] P. Solin, S. K., I. Doležel, *Higher-Order Finite Element Methods*, Chapman & Hall/CRC, Boca Raton, 2003.
- [17] P. Solin, et al. Hermes – Higher-Order Modular Finite Element System. URL <http://hpfem.org/>.
- [18] P. Karban, et al. Agros2d – application for solution of physical fields. URL <http://agros2d.org>.
- [19] P. Solin, J. Červený, I. Doležel, Arbitrary level hanging nodes and automatic adaptivity in the *hp*-fem, *Mathematics and Computers in Simulation* 77 (2008) 117–132.